

# High-flux source of polarization-entangled photons from a periodically poled $\text{KTiOPO}_4$ parametric down-converter

Christopher E. Kuklewicz, Marco Fiorentino, Gaétan Messin, Franco N. C. Wong, and Jeffrey H. Shapiro  
 Research Laboratory of Electronics, Massachusetts Institute of Technology, Cambridge, Massachusetts 02139, USA

(Received 15 May 2003; published 15 January 2004)

We have demonstrated a high-flux source of polarization-entangled photons using a type-II phase-matched periodically poled  $\text{KTiOPO}_4$  parametric down-converter in a collinearly propagating configuration. We have observed quantum interference between the single-beam down-converted photons with a visibility of 99% together with a measured coincidence flux of  $300 \text{ s}^{-1}/\text{mW}$  of pump. The Clauser-Horne-Shimony-Holt version of Bell's inequality was violated with a value of  $2.711 \pm 0.017$ .

DOI: 10.1103/PhysRevA.69.013807

PACS number(s): 42.65.Lm, 03.65.Ud, 42.50.Dv

## I. INTRODUCTION

Entanglement is the basis for fundamental demonstrations of quantum mechanics such as violation of Bell's inequality and tests of local realism [1,2]. Moreover, it is essential to a wide variety of quantum communication applications, including teleportation [3,4] and quantum secret sharing [5], and it can be used for quantum key distribution [6]. A high-flux source of polarization-entangled photons is therefore desirable for practical implementation of a variety of entanglement-based applications. Spontaneous parametric down-conversion (SPDC) in a noncollinearly propagating, angle phase-matched crystal, such as beta-barium borate (BBO), is often used to generate polarization entanglement [7–9]. However, only a small segment of the output cone of the down-converted photons is collectible. Moreover, angle phase matching precludes the use of long crystals for more efficient generation or for narrowband generation in a cavity configuration.

We take a different, yet simple, approach to entanglement generation that is based on periodically poled potassium titanyl phosphate (PPKTP) with collinear propagation of the pump, signal, and idler fields. A periodically poled nonlinear crystal such as PPKTP, with an appropriate grating period, permits efficient three-wave mixing at user-selectable wavelengths within the crystal's transparency window by the technique of quasi-phase-matching (QPM) [10]. Under QPM one can choose to propagate along a principal axis of the crystal, thus avoiding undesirable angle walkoff and permitting collinear propagation in long crystals, which can be utilized in cavity configurations for enhancing down-conversion efficiency and providing high-brightness narrowband outputs [11]. Furthermore, a single-beam configuration of copropagating signal and idler photons simplifies the transport of entangled photon pairs. For the current work we report measurements of single-beam quantum interference with a visibility of up to 99% and Bell's inequality violation from a continuous-wave (cw) PPKTP parametric down-converter.

## II. SINGLE-BEAM ENTANGLEMENT

Figure 1 shows the basic concept of our cw collinearly propagating single-beam SPDC for polarization entanglement. It consists of a length- $L$  type-II phase-matched PPKTP

crystal followed by a length- $L/2$  KTP timing compensator. Consider the probability amplitudes of a single pair of down-converted signal and idler photons that originate, via quantum superposition, from two locations,  $A$  and  $B$ , which are symmetrically displaced from the center of the periodically poled crystal [12]. Because of the crystal's birefringence, the horizontally ( $H$ ) polarized signal photon along the crystal's  $y$  axis always exits the crystal ahead of the conjugate idler photon, which is vertically ( $V$ ) polarized along the crystal's  $z$  axis. The timing compensator in Fig. 1 is a KTP crystal that is oriented similar to the PPKTP crystal but with the  $y$  and  $z$  axes interchanged. Time-resolved signal and idler photon counting before the compensating crystal will collapse the quantum superposition. This will tag the location— $A$  or  $B$ —at which the pair was created by virtue of the time difference between the signal and idler counts. After the compensator, the signal and idler pair is at a quantum superposition of locations  $C$  and  $D$ , with either  $H_A$  leading  $V_A$  or  $V_B$  leading  $H_B$  by the same time interval. The temporal information has been erased because the separation of the photon pair no longer reveals the source location in the PPKTP. Although the timing compensator has erased one feature that distinguishes the signal and idler photons, they are still distinguishable by virtue of their orthogonal polarizations. This polarization information can be erased, however, by rotating the output polarizations by  $\pi/4$ , before analysis along  $H$  and  $V$ . The erasure of such identifying information is essential to all quantum-interference experiments [16]. Furthermore, it is also necessary to erase any frequency or spatial mode information, which might distinguish between photons in a de-

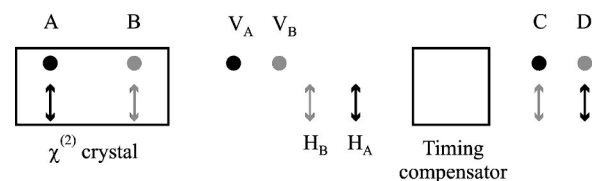


FIG. 1. Schematic for generating entanglement in a single optical beam. A single signal/idler photon pair is generated, via quantum superposition, at locations  $A$  and  $B$ . The timing of the probability amplitudes of the orthogonally polarized outputs from locations  $A$  and  $B$  in a  $\chi^{(2)}$  crystal is shown before and after a timing compensation crystal. Timing information is erased for photon pairs at locations  $C$  and  $D$ . Horizontal (vertical) polarization:  $\uparrow$  ( $\bullet$ ).

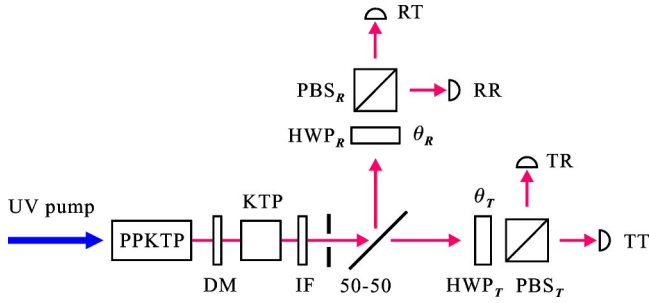


FIG. 2. Schematic of experimental setup. The 50-50 beam splitter is removed for quantum interference measurements which are made with detectors  $TT$  and  $TR$ . Detectors  $TT$  and  $RT$  are used for Bell's inequality measurements. DM, dichroic mirror; IF, interference filter; HWP, half-wave plate; PBS, polarizing beam splitter.

tected pair, by collecting only collinear and degenerate pairs. Ignoring the vacuum and higher photon-number components, the state at the output of this polarization rotation is the biphoton,

$$|\psi\rangle = (|H\rangle_1|H\rangle_2 - |V\rangle_1|V\rangle_2)/\sqrt{2}. \quad (1)$$

The photons labeled 1 and 2 can be analyzed with a polarization beam splitter (PBS) and a null should occur in coincidence measurements. This coincidence null is equivalent to the coincidence dip in Hong-Ou-Mandel (HOM) interferometry [16–18].

It is possible to utilize the single-beam SPDC output of Fig. 1 to obtain polarization-entangled photons with a 50-50 beam splitter. Each photon of the orthogonally polarized photon pair that is generated from the PPKTP is equally likely to be transmitted or reflected at the beam splitter. Hence half of the generated pairs yield one photon in the transmitted path and one in the reflected path. If we postselect only these events within a coincidence window, the two photons in the two paths are in a polarization-entangled triplet state:

$$|\psi\rangle = (|H\rangle_T|V\rangle_R + |V\rangle_T|H\rangle_R)/\sqrt{2}, \quad (2)$$

where the subscripts  $T$  and  $R$  refer to the transmitted and reflected paths of the 50-50 beam splitter, respectively. We note that postselection is not necessary if quantum memories that allow nondestructive loading verification are used [4,19].

### III. SINGLE-BEAM QUANTUM INTERFERENCE

We have implemented the single-beam down-conversion scheme in the setup shown in Fig. 2. A 10-mm-long flux-grown PPKTP crystal with a grating period of  $8.84 \mu\text{m}$  was used for frequency-degenerate type-II quasi-phase-matched operation at a pump wavelength of 397 nm. The output wavelength at 795 nm was chosen to match the transition wavelength of the  $D_1$  line of Rb, which has been proposed for use as a trapped-atom quantum memory for long-distance teleportation [4,19]. The 1-mm-thick PPKTP crystal was antireflection coated at 397 and 795 nm and was pumped with

a 10-mW cw external-cavity ultraviolet (UV) diode laser that was weakly focused to a  $\sim 200\text{-}\mu\text{m}$  beam waist in the crystal. The crystal was set up for collinear propagation along its  $x$  axis and with its  $y$  axis aligned with the pump's horizontal polarization. For type-II phase matching, the nonlinear coefficient  $d_{24}$  was utilized, and the signal and idler outputs were orthogonally polarized along the crystal's  $y$  and  $z$  axes, respectively. The operating temperature of the PPKTP crystal was controlled with a thermoelectric cooler that allowed us to tune the crystal to exact frequency degeneracy and was typically set at  $20^\circ\text{C}$ . After passing through the 5-mm-long KTP timing compensator to erase the timing information, the output beam was sent through an interference filter centered at 795 nm that had a 1-nm bandwidth and 80% in-band transmission. We have imaged the down-converted light through the 1-nm interference filter onto a high-sensitivity charge-coupled device camera, and found this light had a divergence full angle of  $\sim 20$  mrad, in good agreement with theoretical estimates of the external divergence angle for our PPKTP system. Due to our propagation along one of the principal axes in PPKTP, the observed divergence angle of 20-mrad/nm of bandwidth is more than an order of magnitude larger than that for the usual angle phase-matched configuration in BBO for a given crystal length and spectral bandwidth [8].

There were some UV-induced fluorescence photons from the flux-grown PPKTP crystal. These fluorescence photons, estimated to be  $\sim 1000$  (photons/s)/mW of pump generated in a 1-nm bandwidth and collected through a small iris, increased the singles rates by  $\sim 5\%$ . Accidental coincidences caused by them were relatively insignificant in our experiments. We installed two dichroic mirrors that passed the 795-nm outputs but attenuated the UV pump by  $\sim 40$  dB to minimize additional fluorescence from the KTP timing compensator and other optical elements. An adjustable iris was used to control the effective divergence angle of the transmitted beam. A smaller iris increased the depth of field and reduced the spatial resolution of the output photons such that the photons generated from locations  $A$  and  $B$  in Fig. 1 would be spatially indistinguishable. The iris also served to block off-axis, nearly degenerate photon pairs that would not contribute to either quantum interference or polarization entanglement.

For quantum-interference measurements, the 50-50 beam splitter in Fig. 2 was not necessary. Removing this beam splitter improves the conditional detection probability by a factor of two, and we have made measurements with and without it present. With the 50-50 beam splitter present, each output beam was sent through a half-wave plate (HWP), a PBS for polarization analysis, and a clean-up polarizer to eliminate the leakage of horizontally polarized light into the vertically polarized path. Also, prisms were used in the horizontally polarized output paths to reduce accidental counts due to the UV pump. All four PBS outputs were focused on commercial Si single-photon counting detectors, whose detection quantum efficiencies are estimated to be 50–55% at 795 nm and whose dark count rates are less than  $100 \text{ s}^{-1}$ . We then combined the  $\sim 35$ -ns-long electrical pulses from detectors  $TT$  and  $TR$  with AND logic, and both the singles

rates from the detector output pulses and the coincidence rate from the logic pulses were counted. The dead times of our single-photon counters (including the pulse width) were measured to be  $\sim 50$  ns, which is negligible at our operating count rates of  $10^5$  s $^{-1}$  or less. By blocking the pump and measuring the singles and coincidence rates due to different amounts of stray light for the four detectors, we were able to determine the effective coincidence window for each pair of detectors and calibrate the accidental coincidence rates for removal in postdetection data analysis. Typical rates, with the 50-50 beam splitter in place, were 12 000 singles s $^{-1}$ , pair coincidences of 1 200 s $^{-1}$  in a  $\sim 70$ -ns coincidence window, and accidental coincidences of  $\sim 12$  s $^{-1}$  for 10 mW of pump and 1-nm detection bandwidth. The main contribution to the accidental coincidences is the Poisson occurrence of a double pair within the coincidence window in which the signal of one pair and the idler of the other pair are detected [20]. The reliability of the logical AND coincidence detection and the data analysis methodology was checked by comparing it to a high time-resolution (sub-ns) start-stop histogram obtained with a Picoquant TimeHarp 200.

Consider the case without the 50-50 beam splitter and with only the detectors labeled  $TT$  and  $TR$  in Fig. 2 in use.  $PBS_T$  in the transmitted path and the crystal's  $y$  and  $z$  axes were aligned such that if the  $HWP_T$ 's fast and slow axes were also aligned the same way, the signal and idler photons would be separately detected to yield the pair generation rate. When  $HWP_T$  was set at  $\theta_T=0$  to yield zero polarization rotation and the iris was open, we observed a coincidence rate as high as 46 100 s $^{-1}$ , from which we infer a pair generation rate of  $\sim 10^6$  s $^{-1}$  using our 21% conditional detection efficiency. At  $\theta_T=\pi/8$ , the output beam underwent a  $\pi/4$  polarization rotation, and each incident photon had a 50-50 chance of being transmitted or reflected at  $PBS_T$ . For photon pairs that were spectrally, spatially, and temporally indistinguishable, the state after  $HWP_T$  was given by Eq. (1), and quantum interference between the signal and idler of a photon pair occurred, resulting in a reduction in the coincidence rate. When we made the photons distinguishable, by frequency detuning, no quantum interference occurred and a coincidence rate of 50% relative to the zero-rotation rate was observed. With the iris open and  $\theta_T=\pi/8$ , we observed a coincidence rate of 11 800 s $^{-1}$ , corresponding to a visibility  $V=[C(0)-C(\pi/8)]/[C(0)+C(\pi/8)]$  of 59%, where  $C(\theta_T)$  is the coincidence rate at a  $HWP_T$  angle setting of  $\theta_T$ . As we reduced the size of the iris, the effective divergence angle was reduced and the depth of field improved, leading to a reduction in the coincidence rates and an increase in the visibility. We have achieved  $V=97.7\%$  with a 200- $\mu$ m-diameter aperture, corresponding to a divergence full angle of  $\sim 2$  mrad, for the flux-grown PPKTP down-converter.

We have also made similar quantum-interference measurements with a second PPKTP crystal, which was hydrothermally grown and had a grating period of 9.01  $\mu$ m. This 10-mm-long crystal was pumped with the second harmonic of a Ti:sapphire laser centered at 397 nm with a maximum usable power of  $\sim 30$  mW. The tunable UV pump source and the temperature tuning of the PPKTP crystal permitted

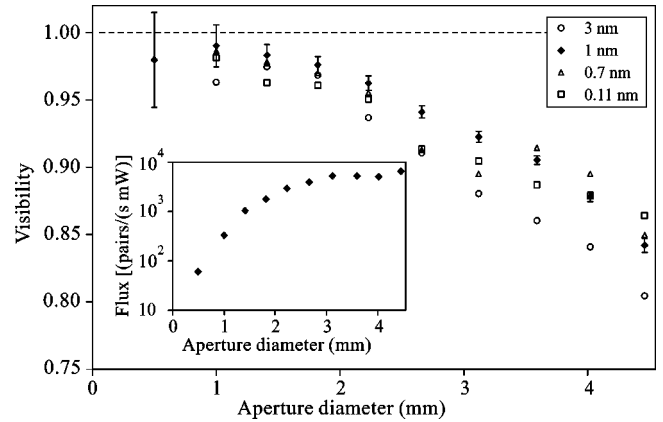


FIG. 3. Plot of visibility  $V$  as a function of aperture diameter for interference filter bandwidths of 3, 1, 0.7, and 0.11 nm. The 0.7-nm filter was composed of two identical 1-nm filters in series. Error bars for the 1-nm data are displayed. The inset plots the detected coincidence flux as a function of the aperture size for the filter bandwidth of 1 nm, showing the trade-off between usable flux and visibility.

us to maintain the SPDC operating point at exact frequency degeneracy for the collinearly propagating portion of the output. Typical pump powers were 5 mW and the crystal temperature was usually set at 30 °C. We added a collimating lens for the output beam and an adjustable iris was used to control the depth of field. The conditional detection efficiency for the hydrothermally grown PPKTP setup was  $\sim 25\%$  for a 3-mm-diameter aperture and a 3-nm interference filter. Figure 3 shows the quantum-interference visibility as a function of the aperture size for four different interference-filter bandwidths. At the aperture size of 1 mm, which is equivalent to a divergence full angle of 5.4 mrad, we observed a visibility of  $99 \pm 1\%$  for the 1-nm filter. Figure 3 clearly shows that for larger aperture sizes, which correspond to shallower depths of field at the crystal, the visibility is reduced. This reduction occurred because spatial and spectral indistinguishability was no longer fully maintained. The inset in Fig. 3 shows the detected coincidence rate as a function of the aperture size for the case of the 1-nm filter. At the highest visibility level of 99%, obtained with a 1-mm aperture, the measured coincidence rate was  $\sim 300$  s $^{-1}$ /mW of pump power, which is one of the highest reported values at near-unity visibility level for an entanglement source [7,8]. Moreover, for an aperture size of 3 mm, with a corresponding divergence angle of 16 mrad, we measured a flux of over 5 000 s $^{-1}$ /mW of pump while maintaining a visibility of 90%. We should note that the hydrothermally grown PPKTP crystal was found to be more efficient (with  $d_{\text{eff}} \sim 1.60$  pm/V) than the flux-grown PPKTP crystal ( $d_{\text{eff}} \sim 0.74$  pm/V). In addition, the UV-induced fluorescence of the hydrothermally grown PPKTP was about 25% of that for the flux-grown crystal.

#### IV. POLARIZATION ENTANGLEMENT

One can easily obtain polarization-entangled photon pairs using the experimental setup in Fig. 2. Each member of an

orthogonally polarized photon pair that is generated in the PPKTP down-converter has a 50% chance of being transmitted or reflected by the 50-50 beam splitter. When one photon appears in the transmitted path and one in the reflected path—something that can be postselected by monitoring for coincidences—the joint state of the beam-splitter's output is the polarization-entangled triplet given by Eq. (2).

The quality of the single-beam polarization entanglement can be evaluated by measuring the violation of the Clauser, Horne, Shimony, and Holt (CHSH) form of Bell's inequality [2]. We have made such Bell's inequality measurements using the diode-pumped flux-grown PPKTP down-converter with a 1-nm interference filter and  $\sim 10$  mW of pump power. Referring to Fig. 2, the light in the transmitted path and in the reflected path of the 50-50 beam splitter were separately analyzed with a HWP and a PBS. Simultaneous coincidence measurements between detectors  $TT$  and  $RT$  ( $C_{TT,RT}$ ), detectors  $TR$  and  $RR$  ( $C_{TR,RR}$ ), and detectors  $TT$  and  $TR$  ( $C_{TT,TR}$ ), as indicated in Fig. 2, were taken for two different  $\theta_T$  settings of 0 and  $\pi/8$  for the transmitted beam. The HWP<sub>T</sub>'s angle setting  $\theta_T$  was ascertained by quantum-interference measurements in the transmitted path using  $C_{TT,TR}$ . At each  $\theta_T$  angle, coincidence measurements  $C_{TT,RT}$  and  $C_{TR,RR}$  over a 10-s interval were taken at 32 different positions of the HWP<sub>R</sub>'s setting ( $\theta_R$  at  $\sim \pi/16$  intervals) in the reflected path of the 50-50 beam splitter. These coincidence measurements were used to calculate the value of the CHSH inequality. Figure 4 shows the coincidence counts  $C_{TT,RT}$  for  $\theta_T=0$  and for  $\theta_T=\pi/8$  and their sinusoidal fits,

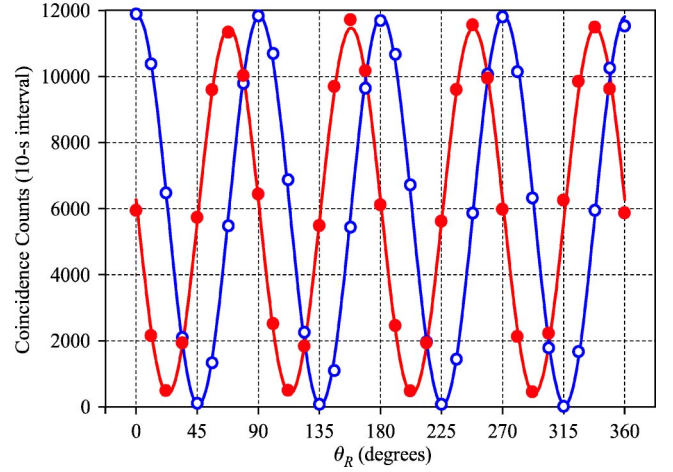


FIG. 4. Plot of coincidence counts for  $\theta_T=0$  (open circles) and  $\theta_T=\pi/8$  (solid circles) in a 10-s counting interval as a function of HWP<sub>R</sub> setting  $\theta_R$  in the reflected path of the 50-50 beam splitter in Fig. 2. Accidental coincidences have been removed in these plots and the sinusoidal fits (solid lines) are used for obtaining visibility and the  $S$  parameter in the CHSH inequality.

showing visibilities of 98% and 93%, respectively.

The four coincidence-count data sets of  $C_{TT,RT}$  and  $C_{TR,RR}$  for  $\theta_T=0$  and  $\theta_T=\pi/8$  are fit to sinusoidal functions. Using these four fits (with their estimated errors) we construct the CHSH expectation  $E$  functions and the  $S$  parameter function [7,9].  $E$  is defined by

$$E(\theta_T, \theta_R) = \frac{C_{TT,RT}(\theta_T, \theta_R) + C_{TR,RR}(\theta_T, \theta_R) - C_{TT,RR}(\theta_T, \theta_R) - C_{TR,RT}(\theta_T, \theta_R)}{C_{TT,RT}(\theta_T, \theta_R) + C_{TR,RR}(\theta_T, \theta_R) + C_{TT,RR}(\theta_T, \theta_R) + C_{TR,RT}(\theta_T, \theta_R)}. \quad (3)$$

Note that  $E$  depends on  $C_{TT,RR}$  and  $C_{TR,RT}$ , which were not directly measured, so we derive their values from the fits of  $C_{TT,RT}$  and  $C_{TR,RR}$  with  $\theta_R \rightarrow \theta_R + \pi/4$ :

$$C_{TT,RR}(\theta_T, \theta_R) = C_{TT,RT}\left(\theta_T, \theta_R + \frac{\pi}{4}\right), \quad (4)$$

$$C_{TR,RT}(\theta_T, \theta_R) = C_{TR,RR}\left(\theta_T, \theta_R + \frac{\pi}{4}\right). \quad (5)$$

The parameter  $S$  is composed of  $E$  functions for two values of  $\theta_R$  and two values for  $\theta_T$ . In our case  $\theta_T=0, \pi/8$  and  $\theta_R=\pi/16, 3\pi/16$ . Thus our  $S$  parameter is defined as

$$S = \left| E\left(0, \frac{\pi}{16}\right) - E\left(\frac{\pi}{8}, \frac{\pi}{16}\right) + E\left(0, \frac{3\pi}{16}\right) + E\left(\frac{\pi}{8}, \frac{3\pi}{16}\right) \right|. \quad (6)$$

Classical and hidden variable theories predict  $S \leq 2$ , while quantum mechanics permits  $S \leq 2\sqrt{2} \approx 2.828$ , with equality occurring for maximal polarization entanglement, i.e., a polarization Bell state such as the triplet from Eq. (2). We ob-

tained an  $S$  value of  $2.711 \pm 0.017$ , which indicates good polarization entanglement of our PPKTP SPDC source.

## V. CONCLUSION

In summary, we have demonstrated a cw high-flux source of polarization-entangled photons using a PPKTP parametric down-converter in a collinearly propagating configuration. The single-beam output is shown to allow easy control of its spatial and spectral contents and simplify the transport of the photon pairs. By using a circular aperture we were able to obtain a high visibility of 99% with a corresponding flux of  $\sim 300$  s<sup>-1</sup>/mW of pump power. Polarization entanglement was obtained from the cw single-beam PPKTP down-converter with a 50-50 beam splitter, and we measured Bell's inequality violation with  $S=2.711 \pm 0.017$ . We have found that the use of periodically poled nonlinear material and the single-beam collinearly propagating configuration offer distinct advantages over the usual noncollinearly phase-matched BBO down-converter. Wavelength tunability of the paired photons with no change in the output beam angle can

be easily accomplished with temperature tuning of the crystal and/or a change in the pump wavelength. Long crystals with collinear outputs can be used to allow more efficient generation and collection of entangled photons. We expect that future entanglement sources based on cavity-enhanced parametric down-conversion in long crystals can significantly improve on its flux and also its spatial and spectral contents [11,15].

## ACKNOWLEDGMENTS

This work was supported by the DoD Multidisciplinary University Research Initiative (MURI) program administered by the Army Research Office under Grant No. DAAD-19-00-1-0177, and by the National Reconnaissance Office. The authors thank Peter Hendrickson for fruitful discussion.

- 
- [1] J.S. Bell, *Rev. Mod. Phys.* **38**, 447 (1966).
- [2] J.F. Clauser, M.A. Horne, A. Shimony, and R.A. Holt, *Phys. Rev. Lett.* **23**, 880 (1969).
- [3] C.H. Bennett, G. Brassard, C. Crépeau, R. Jozsa, A. Peres, and W.K. Wootters, *Phys. Rev. Lett.* **70**, 1895 (1993).
- [4] J.H. Shapiro, *New J. Phys.* **4**, 47. 1 (2002).
- [5] M. Hillery, V. Buzek, and A. Berthiaume, *Phys. Rev. A* **59**, 1829 (1999).
- [6] A.K. Ekert, *Phys. Rev. Lett.* **67**, 661 (1991).
- [7] P.G. Kwiat, E. Waks, A.G. White, I. Appelbaum, and P.H. Eberhard, *Phys. Rev. A* **60**, R773 (1999).
- [8] C. Kurtsiefer, M. Oberparleiter, and H. Weinfurter, *Phys. Rev. A* **64**, 023802 (2001).
- [9] P.G. Kwiat, K. Mattle, H. Weinfurter, A. Zeilinger, A.V. Sergienko, and Y. Shih, *Phys. Rev. Lett.* **75**, 4337 (1995).
- [10] M.M. Fejer, G.A. Magel, D.H. Jundt, and R.L. Byer, *IEEE J. Quantum Electron.* **28**, 2631 (1992).
- [11] J.H. Shapiro and N.C. Wong, *J. Opt. B: Quantum Semiclassical Opt.* **2**, L1 (2000).
- [12] Rigorous treatment of SPDC requires a Gaussian-state description, to properly account for multiple-pair events. We have previously reported [13–15] a Gaussian-state analysis that unifies the principal quantum signatures produced by  $\chi^{(2)}$  interactions. Furthermore, we have shown how the low-gain limit of the polarization-entangled Gaussian state is well approximated by vacuum plus biphoton components [15]. Because our down-converter operates in this low-gain regime, it is appropriate to describe its nonvacuum output component in terms of the probability amplitudes of a biphoton state. Because the biphoton description is more intuitive than the rigorous Gaussian-state characterization, we have chosen to use the former throughout this paper.
- [13] J.H. Shapiro and K.-X. Sun, *J. Opt. Soc. Am. B* **11**, 1130 (1994).
- [14] J.H. Shapiro, *Proc. SPIE* **5111**, 382 (2003).
- [15] J. H. Shapiro, in *Proceedings of the Sixth International Conference on Quantum Communication, Measurement and Computing*, edited by J.H. Shapiro and O. Hirota (Rinton Press, Princeton, 2003), pp. 153–158.
- [16] M.H. Rubin, D.N. Klyshko, Y.H. Shih, and A.V. Sergienko, *Phys. Rev. A* **50**, 5122 (1994).
- [17] C.K. Hong, Z.Y. Ou, and L. Mandel, *Phys. Rev. Lett.* **59**, 2044 (1987).
- [18] C.E. Kuklewicz, E. Keskiner, F.N.C. Wong, and J.H. Shapiro, *J. Opt. B: Quantum Semiclassical Opt.* **4**, S162 (2002).
- [19] S. Lloyd, M.S. Shahriar, J.H. Shapiro, and P.R. Hemmer, *Phys. Rev. Lett.* **87**, 167903 (2001).
- [20] The biphoton state from Sec. II is the leading (first-order) nonvacuum term when the Gaussian state produced by SPDC is expanded in the number-state basis. That  $\sim 1\%$  of our coincidences are due to double-pair occurrences represents the contribution of the second-order term in this number-state expansion. In Ref. [18] we used the Gaussian-state treatment of SPDC to analyze a quantum-interference measurement similar to that of Fig. 2. The same analysis procedure can be used for the Bell's inequality configuration. When the coincidence gate is short enough that the probability of a singles count in that time window is low, then the Gaussian-state results reduce to those obtained from the biphoton description.